Geophys. J. Int. (1996) **125**, 325–339

Rayleigh-wave dispersion along the Hawaiian Swell: a test of lithospheric thinning by thermal rejuvenation at a hotspot

Mark T. Woods* and Emile A. Okal

Department of Geological Sciences, Northwestern University, Evanston, IL 60208, USA

Accepted 1995 October 18. Received 1995 October 10; in original form 1994 September 7

SUMMARY

In this paper we present a seismological test of the 'thermal rejuvenation' model for the formation of the Hawaiian Swell, the archetype of a midplate hotspot swell. Two-station measurements of Rayleigh-wave group and phase velocities between Midway Atoll and O'ahu provide the basis for the test: comparison of the observed dispersion curves with age-dependent, regionalized dispersion curves suggests that the swell has the seismic velocity structure of 50–110 Myr old lithosphere rather than that of 20–50 Myr old lithosphere as suggested by the rejuvenation model. Joint inversion of the group- and phase-velocity curves for isotropic velocity models yields an estimate of ~100 km for the seismic lithosphere's thickness along the swell. This value is difficult to reconcile with the 40–50 km thickness demanded by the rejuvenation model. Preliminary measurements of the coefficients of anelastic attenuation are also presented. Although the accuracy of these values is difficult to assess, they too appear to be consistent with thick lithosphere.

Key words: hotspots, oceanic lithosphere, Rayleigh waves.

INTRODUCTION

The Hawaiian Swell in the north Pacific Ocean is a broad, shallow region that extends from the island of Hawai'i to Midway Atoll. It is about 2100 km long, 1200 km wide, and stands about 1.5 km above the surrounding abyssal plain (Fig. 1). Betz & Hess (1942) were the first to recognize both its size and tectonic significance, and they suggested that the swell and the volcanic archipelago situated on its crest originated as fissure eruptions along transcurrent faults that had resulted from stresses in the Pacific Basin. Although this hypothesis has occasionally been re-examined and modified within the framework of plate tectonics (e.g. Jackson & Wright 1970; McDougall 1971; Jackson & Shaw 1975), the consensus has been that the chain of islands and seamounts was formed by the passage of the Pacific Plate over a stationary mantle plume (Wilson 1963; Morgan 1971, 1972). Indeed, the Hawaiian–Emperor Chain is the archetype of a midplate hotspot track, as distinct from aseismic ridges, such as the Nazca Ridge and the Walvis Ridge, which are generated at or near an active oceanic spreading centre. [Clague & Dalrymple (1989) recently reviewed alternative hypotheses for the origin of the Hawaiian Chain.]

The mechanism that generates the associated bathymetric swell remains, however, problematic. The purpose of this paper is to test one commonly accepted model, lithosphere thinning via thermal rejuvenation, by examining Rayleigh-wave group velocities, phase velocities, and anelastic attenuation along the swell. It thus extends the preliminary results of Woods *et al.* (1991), which suggested that group velocities along the swell's longitudinal axis are incompatible with the values predicted by the 'thermal rejuvenation' model.

In the rejuvenation model, which was first proposed by Detrick & Crough (1978), the underside of the lithosphere is heated by a mantle plume. The isotherm that defines the lithosphere is therefore deflected upwards, so that the lithosphere above the plume is effectively thinned (Fig. 2). At a given depth, asthenosphere replaces lithosphere, and because the vertically integrated density structure has been changed, the ocean floor rises isostatically, forming the swell. As the plate then moves past the plume it cools, and the swell subsides following the subsidence curves established for lithosphere newly formed at spreading centres (e.g. Menard 1973; Parsons & Sclater 1977).

A variety of geophysical observations have been thought to support the rejuvenation model. In the case of the Hawaiian Swell, its geoid and gravity signatures (e.g. Crough 1978, 1983; Sandwell & Poehls 1980; Sandwell & Renkin 1988), its shape and subsidence rate (e.g. Detrick & Crough 1978; Menard & McNutt 1982; Epp 1984), and its heat flow (e.g. Detrick *et al.* 1981; Von Herzen *et al.* 1982) have all been taken as evidence in support of the model. Estimates of the thinning required to explain these observables indicate that the lithosphere can

* Now at: HQ AFTAC/TTR, 1030 S. Highway A1A, Patrick AFB, FL 32925–3002, USA.

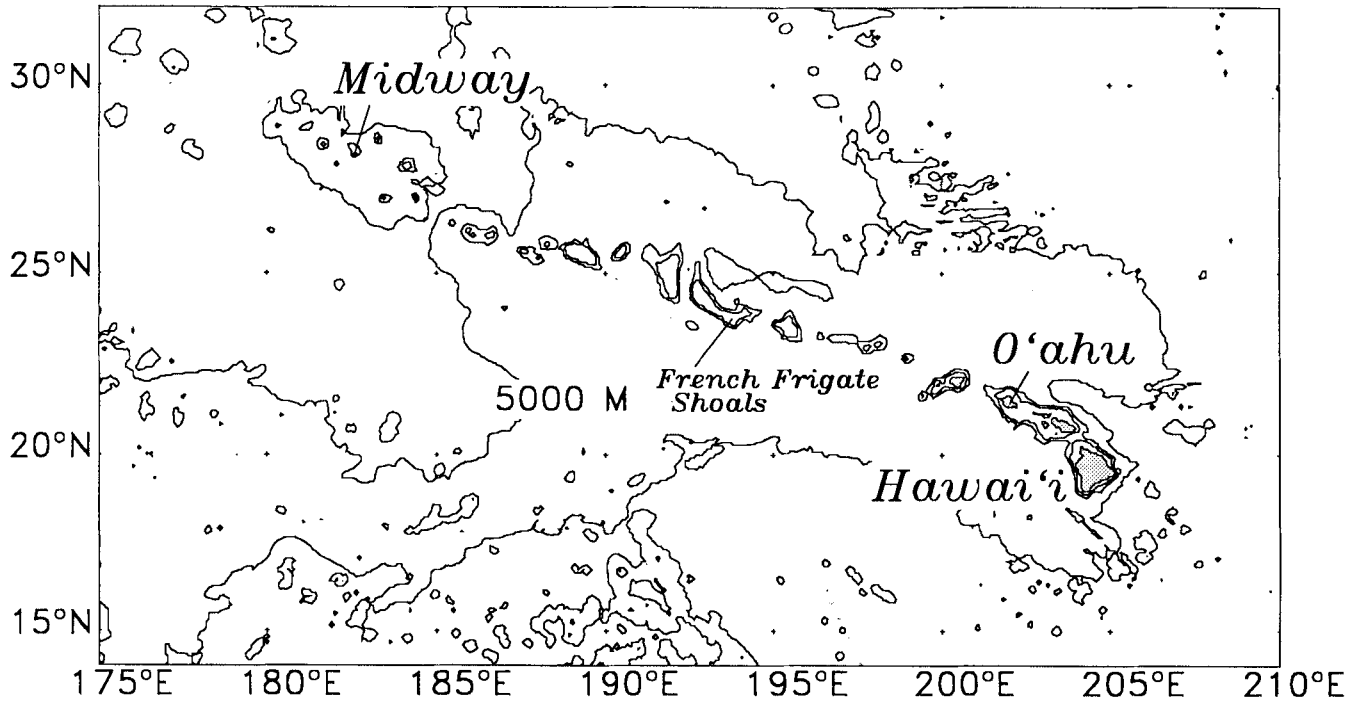

Figure 1. Mercator projection of the study area constructed from DBDB5 digital bathymetric data (US National Oceanographic Office 1985). The Hawaiian Swell is delineated here by the 5000 m isobath. Note the extremes of bathymetry along the Hawaiian Chain, exemplified by the deep area immediately north of French Frigate Shoals. Data from seismograph stations on Midway Atoll and O'ahu are used in this study.

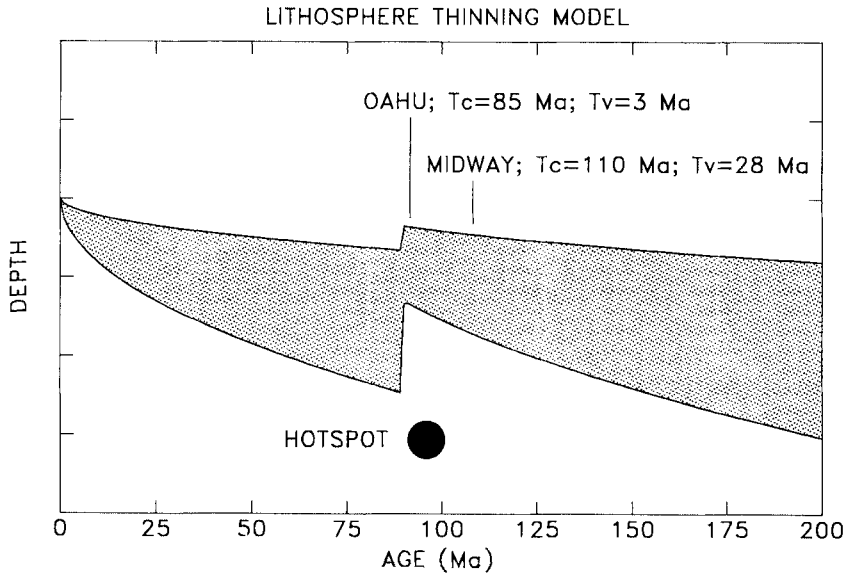

Figure 2. Schematic diagram of the 'thinning by thermal rejuvenation' model for the formation of midplate hotspot swells. Hot lithosphere is created at the spreading centre (zero-age). As it moves away from the spreading centre it cools conductively, so it subsides and thickens (values for depth and thickness depend on various model parameters, so, for generality, none is shown here). As the plate passes over the hotspot, it is reheated and thinned, thereby reacquiring the mechanical and thermal characteristics of younger lithosphere. The ages of oceanic crust (t_c) and volcanic edifices (t_v) are shown for O'ahu and Midway.

only be ~40–50 km at the hotspot (e.g. Crough 1978; Von Herzen *et al.* 1982).

Perhaps the most definitive test of the model, suggested by Detrick & Crough (1978), depends on seismic surface waves. Because surface-wave observables depend strongly on the rigidity of the propagation medium, they are controlled largely by the temperature structure and thickness of the oceanic lithosphere (e.g. Forsyth 1975; Leeds 1975). Thus, they provide insight into the depth of the boundary between the seismic lithosphere and the asthenosphere, which is the key to understanding whether the swell has been produced by thermal rejuvenation and thinning or by another process, such as the dynamic uplift envisioned by Morgan (1972). Because surface waves commonly have wavelengths from 80 to 400 km, they

sample the crust and upper mantle and so provide useful tools with which to determine lithospheric thickness.

Until recently, however, the suggested surface-wave test of the rejuvenation model had not been possible. Isolating the dispersion characteristics of the Hawaiian Swell requires two-station measurements, but seismograph stations had existed only at its south-eastern end, on O'ahu and on Hawai'i. Therefore, in 1989, in collaboration with the Institut de Physique du Globe in Strasbourg, France, we installed a broad-band seismic station on Midway Atoll (MWY) near the north-western end of the Hawaiian chain. Consisting of Streckeisen STS-1 vertical and horizontal seismometers, with a digital data-logger configured as in the French GEOSCOPE network, the station provided good data despite the usual noise problems associated with small island sites. Using waveforms recorded at this station and at existing stations on O'ahu, the test proposed by Detrick & Crough became possible.

EXPERIMENTAL DESIGN

Selection of propagation paths

Because sampling a structure with a characteristic length l requires waves with wavelength $\lambda \leq l$, it is important to consider the size of the Hawaiian Swell before selecting propagation paths for this investigation. The great-circle distance between MWY and the two seismograph stations on O'ahu, KIP and HON, is about 2100 km. The observed half-width of the swell is about 600 km. This value is probably larger than the plume's radius of influence on the lithosphere; some recent numerical models of the swell use radii (2-σ width of Gaussian-shaped, axisymmetric temperature perturbation) of 450–550 km (e.g. Liu & Chase 1989; Zhu & Wiens 1991). Thus, propagation paths from Midway to O'ahu subtending an angle of $\sim 13°$ would be likely to sample the perturbed velocity structure hypothesized to lie beneath the swell. To ensure that the waveforms to be studied traversed this zone, we selected only those paths for which the difference in propagation azimuth to the stations at either end of the swell, δAZM, was less than 2° (Table 1). The great-circle propagation paths are illustrated in Fig. 3, where paths 2, 3, and 4 are seen to lie virtually along the swell's longitudinal axis. Only path 1 is slightly off the axis, but, with $\delta AZM = 1.8°$, it still satisfies the selection criterion.

Given that the local wave vectors **k** of the Rayleigh waves were essentially parallel to the swell, the question is whether their wavelengths were short enough to resolve the structure in both the horizontal and vertical directions. The answer to this question appears to be yes. Consider a representative period, say $T = 40$ s. The phase velocity, C, at this period, for crustal age ranging from 20 to 110 Ma, varies by less than 3 per cent ($3.969 \leq C \leq 4.065$ km s^{-1}, Nishimura & Forsyth 1988), so the wavelength, λ, varies as $159 \leq \lambda \leq 163$ km.

In the horizontal direction, these wavelengths are only about 30 per cent of the radius of influence of the hypothesized plume, so they almost certainly sample the zone where the velocity perturbations are thought to be strongest. Because the swell is a relatively narrow structure, however, the wavefronts propagating along its axis might be distorted, and the apparent velocities measured there could be biased by the influence of the unperturbed structure outside the low-velocity channel. Maupin (1992) showed that, for such scenarios, the measured phase velocities should fall between the values for the unperturbed and rejuvenated oceanic lithospheres. As we shall demonstrate later, such an effect is not observed.

In the vertical direction, the wavelengths for $T = 40$ s sample the depth (50–60 km) at which the lithosphere is presumed to have been replaced by partially molten asthenosphere. (The maximum sensitivity of phase velocity to perturbations in shear velocity, i.e. $\partial C/\partial \beta$, is in this depth range also.) Thus, Rayleigh waves at this period should offer information about the state of rigidity at depth along the swell. At a longer period, say 100 s, the wavelength is longer, ~ 408 km, but it is still smaller than the hypothesized plume radius. Observations at this period should still offer useful information, albeit with degraded resolution.

Possible bias in velocity measurements due to lateral refraction

In the presence of strong lateral velocity contrasts, surface-wave propagation paths may deviate significantly from the ideal great circle from source to receiver. Along the Hawaiian Swell, which is hypothesized to be a low-velocity channel, it is possible that the Rayleigh waves arriving at either MWY or KIP might not have travelled down the channel's axis, but instead might have been refracted into the channel after having travelled most of the interstation distance at high velocity outside the channel.

However, two observations argue against the possibility of lateral refraction and for arrival along the great circle. First, rotation of NS and EW seismograms to the great-circle azimuth effectively separates the surface waves into radial and transverse components. Second, plots of Rayleigh-wave particle motion made using the vertical and calculated radial components of ground motion exhibit clear, retrograde ellipses.

For example, in Fig. 4 the KIP horizontal components for event 2 (1989 Jan 28) are rotated through a range of azimuths in 15° increments, starting with $AZM = 71°$ and ending with $AZM = 161°$. Note that the great-circle value, $AZM = 116°$, separates the energy into radial and transverse components

Table 1. Earthquakes used in this study.

Path	Date	Origin Time	Lat. °N	Lon. °E	M_s	δAZM	Station Pair
1	89 Jan 19	03:17:48.1	-4.03	-105.86	5.8	1.8	HON-MWY
2	89 Jan 28	07:26:54.4	33.01	141.86	5.6	0.7	MWY-KIP
3	89 Sep 05	11:25:56.3	29.45	128.64	5.8	0.6	MWY-KIP
4	89 Sep 05	13:03:37.0	29.52	128.58	5.4	0.5	MWY-KIP

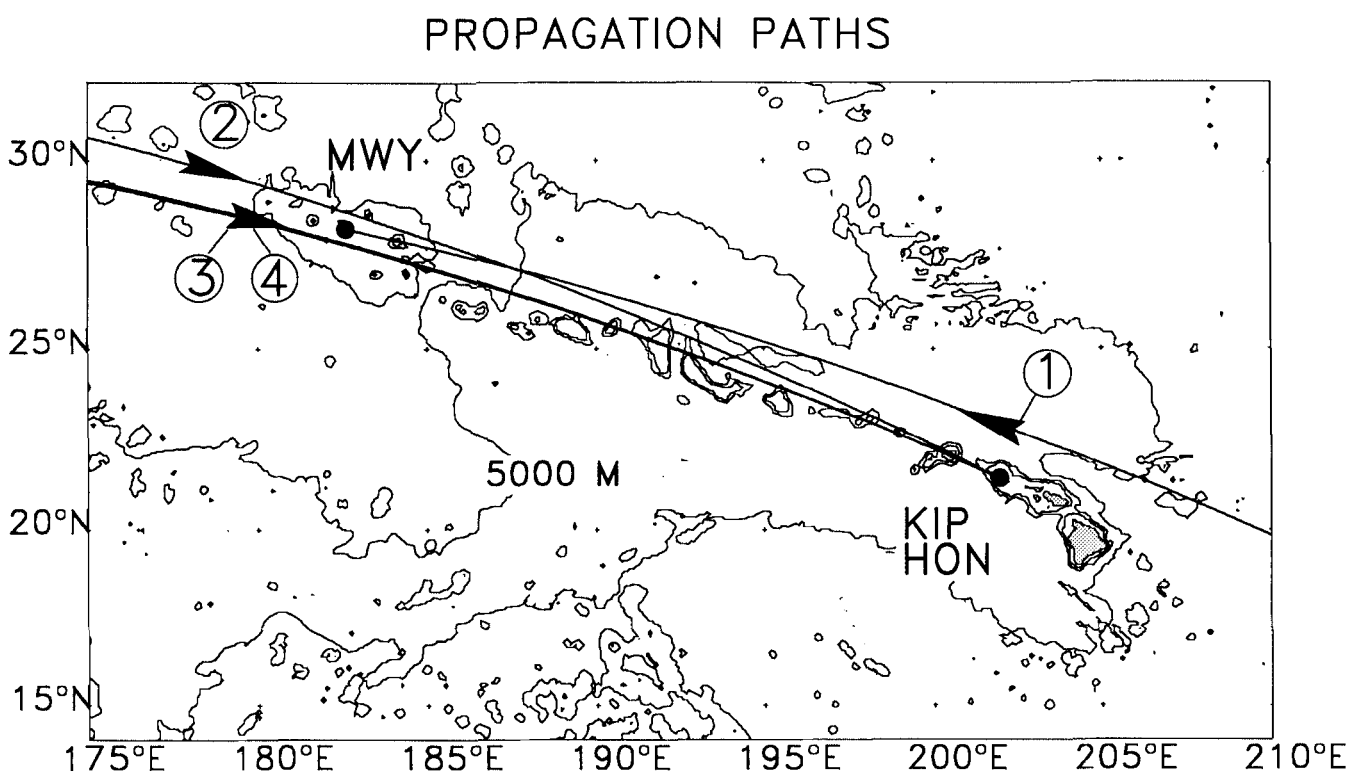

Figure 3. Propagation paths of waveforms used in this study. Path numbers correspond to entries in Table 1. Note that the azimuth of each path is within 2° of the ideal great circle connecting MWY and KIP, and that three paths cross the swell from NW to SE whereas one path crosses the swell from SE to NW.

most effectively. On the transverse component for that azimuth, the Rayleigh-wave amplitude is minimized, although some residual particle motion remains. Moreover, there is no evidence for significant energy arriving either earlier or later than the fundamental Love or Rayleigh modes.

In Fig. 5, elliptical Rayleigh motion is evident, although it is noisy and it appears to have been distorted by the anisotropic fabric of the oceanic lithosphere (Kirkwood & Crampin 1981a, b). In particular, the major axis of the ellipse is tilted away from the vertical, and the ratio of the amplitudes of the semi-major and semi-minor axes ranges between 1.13 and 1.25, rather than the value of 1.47 for a Poisson solid. Such distortion of the particle motion at MWY could be studied to constrain the local extent and orientation of anisotropy (e.g. Vig & Mitchell 1990), but the data base of good horizontal records is not sufficiently extensive to conduct a thorough investigation.

Possible bias in velocity measurements due to clock errors

The inclusion of path 1 (1989 January 19) is important to this investigation because it provides waves that propagated SE to NW. The group and phase velocities derived from this waveform were consistent with the values derived from the other paths, where the energy propagated NW to SE. Because any clock error, δt, would increase the velocity measured in one direction while decreasing it in the other, we are confident that our velocity measurements are not biased in this way.

SURFACE-WAVE ANALYSIS

In our preliminary study of the Hawaiian Swell (Woods *et al.* 1991), we calculated interstation group velocities for the four events listed in Table 1 by applying multiple-filter analysis (MFA) and phase-match filters (PMF) to the interstation cross-correlograms of the digital seismograms. In this paper, we extract three observables, group velocity, U, phase velocity, C, and the coefficient of anelastic attenuation, γ, from displacement seismograms using the above techniques in conjunction with a frequency-domain Wiener filter algorithm (Taylor & Toksöz 1982; Hwang & Mitchell 1986).

Deconvolution of instrument response

The processing sequence for the four events began by removing the instrument response from the digital signals. To eliminate high- and low-frequency noise, we applied a cosine taper and filter to the spectra, passing frequencies between 0.002 and 0.04 Hz. This filter yielded clear, long-period surface waves, free from beats or other apparent interference. It also excluded from the waveforms those short-period components that contain information about crustal thickness, but this value is available from the many refraction and reflection surveys of the Hawaiian Ridge (e.g. Furumoto *et al.* 1968; Furumoto, Campbell & Hussong 1971; Lindwall 1988). Clear, longer-period surface waves that sample the depth range 30–100 km are more important to the present study.

Modal isolation with phase-match filters

The second step in the processing sequence was the application of PMF (Herrin & Goforth 1977; Russell, Herrmann & Hwang 1988) to the individual signals. Unlike in Woods *et al.* (1991), our goal at this stage was not to calculate phase and group

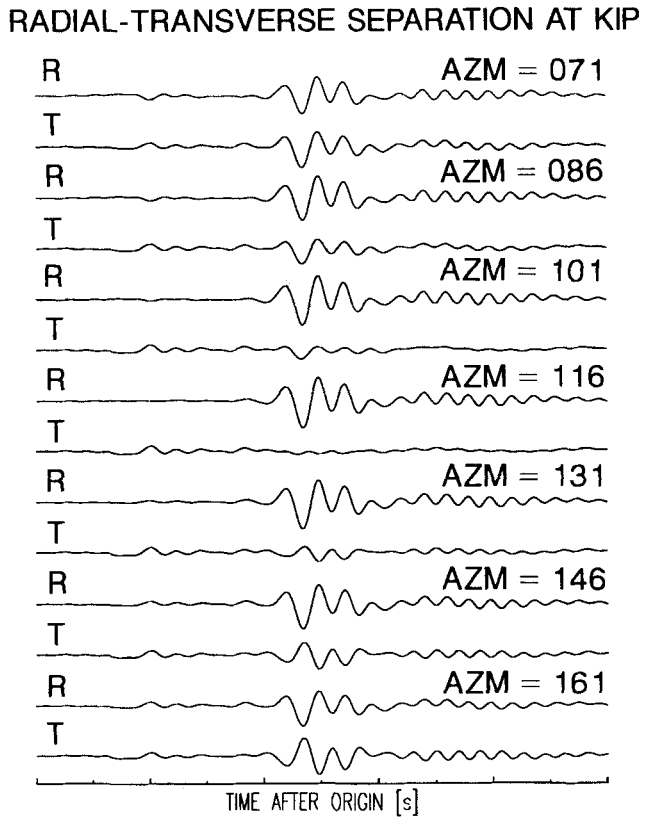

Figure 4. Summary of the test for lateral refraction of a surface wave arriving at KIP. Horizontal components (radial and transverse) are rotated through a total of 90° in 15° increments. Numbers correspond to the azimuth of projection. Note that with $AZM = 116°$, the calculated great-circle value, the radial and transverse components separate the Love and Rayleigh waves very effectively.

velocities (which would be source-to-receiver rather than interstation values), but to extract the best estimates of noise-free, fundamental-mode Rayleigh waveforms. Isolation of the mode of interest is important because Wiener filters cannot remove the effects of overtones (Hwang & Mitchell 1986). Moreover, having signals with smooth amplitude spectra is crucial to the measurement of γ. We allowed for a 10 per cent bias in the estimated amplitudes due to spectral curvature, and used for the required pilot dispersion curve the results of Nishimura & Forsyth (1988) for lithosphere with crustal age varying as $52 \leq t_c \leq 110$ Myr.

Wiener filter extraction of interstation Green's function

The final step in the processing sequence was to use Wiener filters to construct the best estimate of the interstation Green's function, or path response P, from which U, C, and γ can be obtained. Where $H(f)$ is the frequency-domain representation of a signal and $H^*(f)$ is its complex conjugate, we computed

$$P(f) = \frac{H^*_{\mathrm{MWY}}(f)\, H_{\mathrm{KIP}}(f)}{H^*_{\mathrm{MWY}}(f) H_{\mathrm{MWY}}(f)}, \tag{1}$$

where the numerator is the cross-correlation of the waveforms recorded at the two stations, and the denominator is the autocorrelation of the waveform at the station which is closer to the source (here taken as MWY). By windowing the auto- and

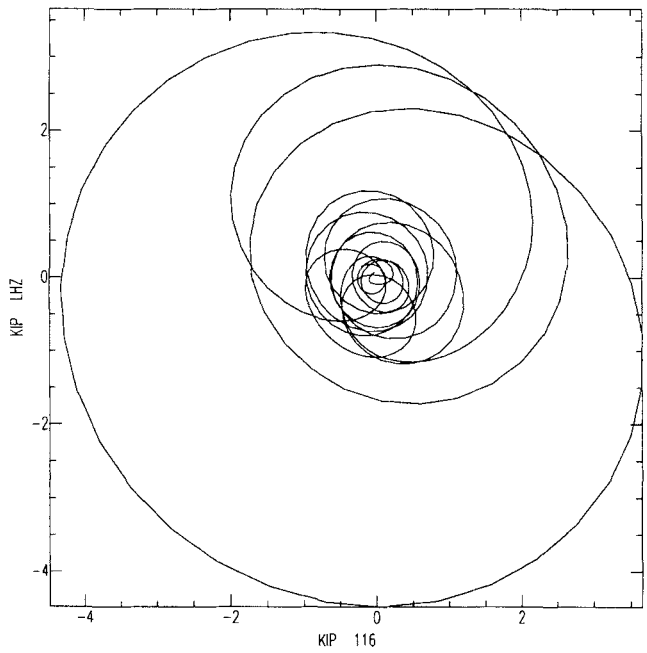

Figure 5. Rayleigh-wave particle motion in the 'sagittal' plane, reconstructed by plotting the vertical component of motion against the radial component ($AZM = 116°$). A clear retrograde ellipse is evident, but the semi-major axis is tilted away from the vertical by the effects of anisotropy.

cross-correlograms with trapezoidal windows, we smoothed any remaining nulls in the spectra so that eq. (1) remained stable. The path responses are illustrated in Fig. 6.

The velocities and attenuation values were then calculated from the path responses. Group velocities, U, were obtained by applying MFA to $P(f)$. Phase velocities, C, were computed using

$$C(f) = \frac{2\pi f x}{2\pi f t_0 + \phi(f) \pm 2n\pi}, \tag{2}$$

where x is the interstation distance in kilometres, and ϕ is the unwrapped, differential phase spectrum of the cross-correlogram. The spatial attenuation coefficients, γ, were calculated with

$$\gamma(f) = \frac{-\ln\left[\,|P(f)|\sqrt{\sin \Delta_{\mathrm{KIP}}/\sin \Delta_{\mathrm{MWY}}}\,\right]}{x}. \tag{3}$$

The results from the group- and phase-velocity calculations for each event were very consistent with one another, so they were averaged and are presented in the next section. For a variety of reasons discussed later, the attenuation measurements were stable only for Event 2 (1989 January 28), and so only those values are presented.

SURFACE WAVE RESULTS

Group and phase velocities

The mean interstation values of U and C calculated from the four waveforms are listed in Table 2 and are illustrated in Fig. 7. Note that the group velocities are about 0.7 per cent

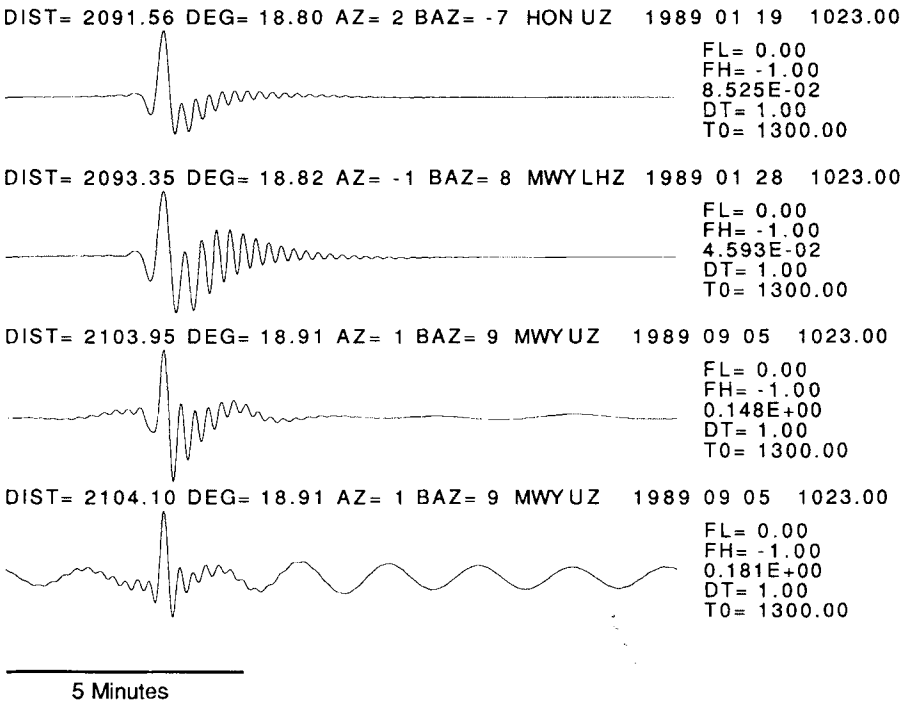

Figure 6. Interstation path responses (Green's functions) computed using Wiener filters. Labels follow the following convention. *DIST*: source–receiver distance in km; *DEG*: source–receiver distance in arc-degrees; *AZ* and *BAZ*: azimuth and back-azimuth; station; date; number of samples; *FL* and *FH*: corner frequencies for display filters; peak amplitude; *DT*: sample interval; T_0: time in s of first sample after origin time.

Table 2. Mean group and phase velocities. Midway-O'ahu.

Period (s)	U (km s^{-1})	*Std.Error* (km s^{-1})	C (km s^{-1})	*Std.Error* (km s^{-1})
30.1	4.026	0.057	4.055	0.017
31.0	4.040	0.051	4.056	0.016
32.0	4.053	0.046	4.056	0.016
33.0	4.065	0.041	4.056	0.015
34.1	4.077	0.037	4.055	0.014
35.3	4.088	0.033	4.054	0.013
36.6	4.097	0.029	4.053	0.013
37.9	4.105	0.025	4.051	0.012
39.4	4.110	0.022	4.049	0.012
41.0	4.113	0.019	4.047	0.012
42.7	4.114	0.016	4.044	0.011
44.5	4.112	0.014	4.041	0.011
46.5	4.108	0.011	4.038	0.011
48.8	4.102	0.009	4.034	0.011
51.2	4.092	0.006	4.031	0.012
53.9	4.081	0.005	4.029	0.012
56.9	4.066	0.006	4.026	0.012
60.2	4.048	0.008	4.024	0.013
64.0	4.027	0.013	4.023	0.014
68.3	4.003	0.018	4.024	0.014
73.1	3.976	0.024	4.026	0.015
78.8	3.945	0.031	4.032	0.016
85.3	3.912	0.038	4.040	0.018

faster than reported in Woods *et al.* (1991), and that the error estimates decrease sharply with period until $T \sim 55$ s, after which they increase slightly. This pattern probably reflects the difficulty of the MFA in handling the steep curvature of the path responses' amplitude spectra, especially at shorter periods. In contrast, the error estimates of the phase velocities are nearly uniform across the pass-band.

Comparison of the interstation measurements with regionalized dispersion curves established by pure-path analyses of large suites of Rayleigh waves that travelled through provinces of the Pacific Ocean Basin with different ages confirms our preliminary results, which indicated that the dispersion characteristics along the Hawaiian Swell are consistent with those for unperturbed, mature oceanic lithosphere. This observation is contrary to our original expectations based on the rejuvenation model, and therefore demonstrates that the model fails the suggested seismological test.

In Fig. 7, four such pure-path curves are illustrated. The lower two curves are characteristic of oceanic lithosphere whose crustal age, t_c, varies as $20 \leq t_c \leq 50$ Myr; the upper two are characteristic of oceanic lithosphere for which $50 \leq t_c \leq 110$ Myr. In each set of curves, the lower one consists of *isotropic* pure-path values (Mitchell & Yu 1980), and the upper one consists of *anisotropic* values (Nishimura & Forsyth 1988), calculated for the azimuth of the great circle connecting MWY and KIP. For this investigation, the dispersion characteristics of the illustrated age provinces discriminate between thermally rejuvenated and unperturbed oceanic lithosphere.

For example, based on the distribution of crustal ages along the Hawaiian Swell, the group and phase velocities should be consistent with the reference curves for older lithosphere. From sea-floor magnetic lineations (Cande *et al.* 1989), t_c near O'ahu is ~85–95 Ma, the uncertainty being due to the proximity of the Moloka'i fracture zone. The crustal age near Midway is ~110 Ma. The ages along the swell vary, therefore, as $85 \leq t_c \leq 110$ Ma. This range is towards the upper bound of the older regionalized dispersion curves.

The rejuvenation model predicts, however, that the group

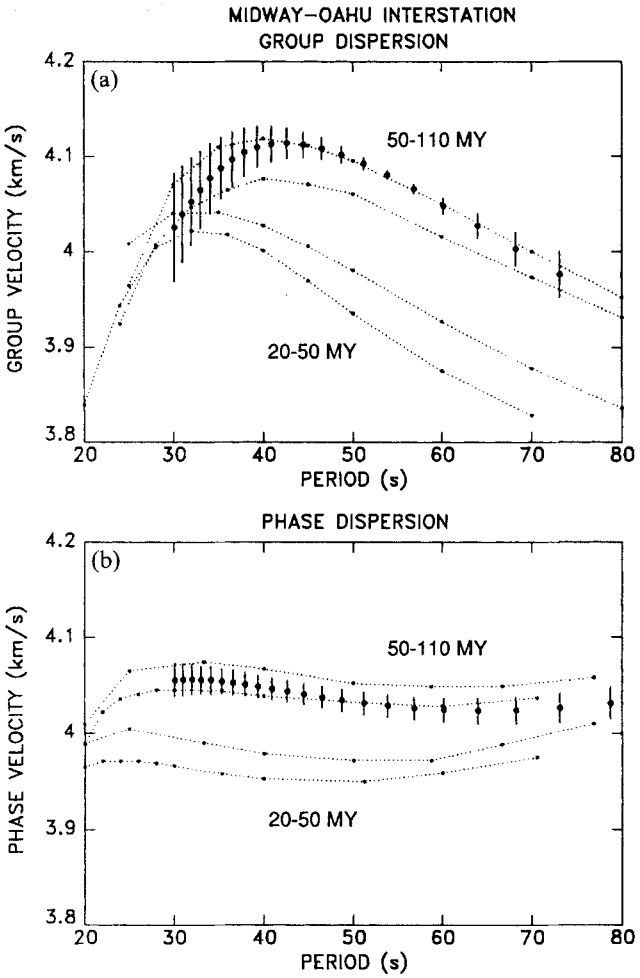

Figure 7. Summary of velocity dispersion test. Measured velocities (filled circles) are compared with pure-path reference dispersion curves (dotted lines). Four references curves are illustrated: the lower two are for oceanic lithosphere whose age varies as $20 \leq t \leq 50$ Myr; the upper two curves are for age $50 \leq t < 110$ Myr. In each pair of reference curves, the lower one represents *isotropic* velocities, and the upper one represents *anisotropic* values along the MWY–KIP azimuth. Error bars represent one standard error. (a) Interstation group-velocity dispersion. (b) Interstation phase-velocity dispersion.

and phase velocities should instead be consistent with the reference curves for younger lithosphere, because the lithosphere's *thermal* age, t_{th}, is presumed to have been reset when it passed over the hotspot. In Crough's (1978) model formulation, oceanic lithosphere acquires the thermal and mechanical characteristics of 25 Myr old lithosphere during this passage. Therefore, the 3 Ma K–Ar age of O'ahu's volcanic shield (Doell & Dalrymple 1973) implies that $t_{th} = 28$ Ma. Similarly, the radiometric age of the volcanic edifice underlying Midway is 28 Ma (Dalrymple, Clague & Lanphere 1977), which in turn implies that $t_{th} = 53$ Ma. The variation of predicted thermal ages, $28 \leq t_{th} \leq 53$ Ma, nearly matches the bounds of the younger of the regionalized dispersion curves. However, the variation would overlap the older regionalized curves if the rejuvenation age were not 25 Myr, but 45 Myr as Wessel (1993) has argued. For this case, the thermal age along the swell varies as $48 \leq t_{th} \leq 73$ Ma, so surface waves probably could not discriminate between perturbed and unperturbed lithosphere. If the rejuvenation age is indeed 45 Myr, then the lithospheric thickness, h_l, has been reduced by only about 30 per cent, whereas the reduction is closer to 50 per cent in Crough's classical formulation.

In any case, if we assume the rejuvenation age to be 25 Myr, these comparisons suggest that surface-wave velocity dispersion along the Hawaiian Swell depends on t_c, rather than on t_{th}. It is difficult, however, to address the question of the depth to which the fast direction of lithospheric anisotropy might have been reset by the hotspot with the current data. For example, the group velocities appear to fit the anisotropic curve for the MWY–KIP path, especially for $T \geq 40$ s, but the phase velocities are on average 0.5 per cent slower than the anisotropic curve.

Attenuation coefficients

As mentioned above, the measurements of γ proved to be stable only for event 2 (1989 January 28). They failed for event 1 because the data used from the DWWSSN station HON have too narrow a pass-band; the longer-period spectral levels ($T > 40$ s) were too strongly attenuated. The situation for events 3 and 4 was more perplexing: even after the PMF the long-period spectra remained slightly noisy, so that the attenuation values oscillated in magnitude and sign.

The stable γ measurements (Table 3) are, however, consistent with the values expected for mature, thick oceanic lithosphere. In Fig. 8, we plot two estimates of γ from the waveforms of event 2 against two pure-path attenuation dispersion curves from Canas & Mitchell (1978). The filled circles are the results of applying eq. (3) to the amplitude spectra of the calculated interstation path response, and the open circles are the results of applying eq. (3) to the individual spectra of the MWY and KIP waveforms. The pure-path curves represent the attenuation that is characteristic of lithosphere for which $0 \leq t_c \leq 50$ Myr and for which $50 \leq t_c \leq 100$ Myr, so again, the pure-path curves provide a diagnostic test of the rejuvenation model. Although the interstation measurements display scatter, they are generally within the error limits for the older pure-path attenuation curve.

Until these values can be verified with measurements from other events, it is difficult to assess their accuracy. As seen in Fig. 8, the estimates from this event vary by as much as 10 per cent at $T \sim 45$ s. However, that clear trends are apparent, and that the trends are generally consistent with one another, encourages us to think that further investigation of attenuation will yield useful results.

INVERSION FOR MODELS OF SHEAR VELOCITY

The availability of both group- and phase-velocity dispersion curves in this investigation allows joint inversion for the shear-velocity structure along the Hawaiian Swell. Although U and C are not independent, inverting them jointly often improves the resolution of the resulting velocity model because the partial derivatives $\partial U(T)/\partial\beta(z)$ and $\partial C(T)/\partial\beta(z)$ have different shapes and sensitivities (Der & Landisman 1972). The first of the five models presented here follows the philosophy of our preliminary study, testing the rejuvenation hypothesis by first coarsely discretizing the model space as a 50 km thick lithosphere overlying a broad low-velocity zone (LVZ) and then

Table 3. Anelastic attenuation coefficients Midway-O'ahu.

Period (s)	γ_{wf} ($\times 10^{-4}$ km^{-1})	Period (s)	γ_{wf} ($\times 10^{-4}$ km^{-1})
---	---	30.1	0.88
---	---	31.0	0.88
---	---	32.0	0.87
---	---	33.0	0.88
---	---	34.1	0.88
---	---	35.3	0.89
---	---	36.6	0.90
37.7	0.81	37.9	0.91
39.2	0.93	39.4	0.92
40.8	1.05	41.0	0.94
42.4	1.13	42.7	0.96
44.1	1.18	44.5	0.98
45.8	1.20	---	---
47.6	1.19	46.5	1.00
49.5	1.15	48.8	1.01
51.5	1.11	51.2	1.03
53.6	1.08	53.9	1.05
55.7	1.04	56.9	1.06
57.9	0.98	---	---
60.2	0.93	60.2	1.07
62.6	0.90	---	---
65.1	0.86	64.0	1.08
67.7	0.84	68.3	1.08
70.4	0.84	---	---
73.2	0.87	73.1	1.07
76.1	0.92	---	---
79.1	0.92	---	---
82.3	0.94	---	---
85.5	0.89	---	---
89.0	0.80	---	---

calculating the changes in the shear velocity structure required to match the velocity observations. In the subsequent four models, we attempt to determine the best estimate of lithospheric thickness, h_l, by following the philosophy of Woods & Okal (1994). In this procedure, the model space is first discretized as a stack of flat, relatively thin (15 km) layers, each with uniform, isotropic velocity. Inverse models constructed in this way suggest the details of the velocity structure demanded by the dispersion curves but without assumptions of where discontinuities might be. Thereafter, by combining those model layers that have similar velocities, simpler, unbiased models can be constructed.

A priori constraints

Knowledge of three physical parameters helps constrain the velocity inversions: the average ocean depth, h_o, the average crustal thickness, h_c, and the crustal velocity, β_c, along the swell. As these have been measured independently of this study, they constitute *a priori* information and were incorporated into the inverse models by a weighting scheme that either keeps these values fixed, or allows them to vary only slightly.

The bathymetry of the Hawaiian Swell is rugged, so estimating h_o along the propagation paths is a problem because it varies over horizontal distances comparable to the wavelengths being studied. For example, the volcanic chain, which is topographically high, sits in a relatively shallow ($\sim$700 m) moat superimposed on the swell. In isolated places, such as immediately north of French Frigate Shoals, the moat's depth exceeds 5 km. Although the 30 s lower band limit of the dispersion curves reduces the influence of ocean depth on the shear-velocity models presented here, a robust estimate of depth minimizes the trade-offs possible between h_o and h_c. We therefore averaged DBDB5 (US Naval Oceanographic Office 1985) values in the rectangle bounded by 20°N, 28°N, 158°W and 178°W to obtain $h_o \sim 4.5$ km. This value was fixed in all of the inversions.

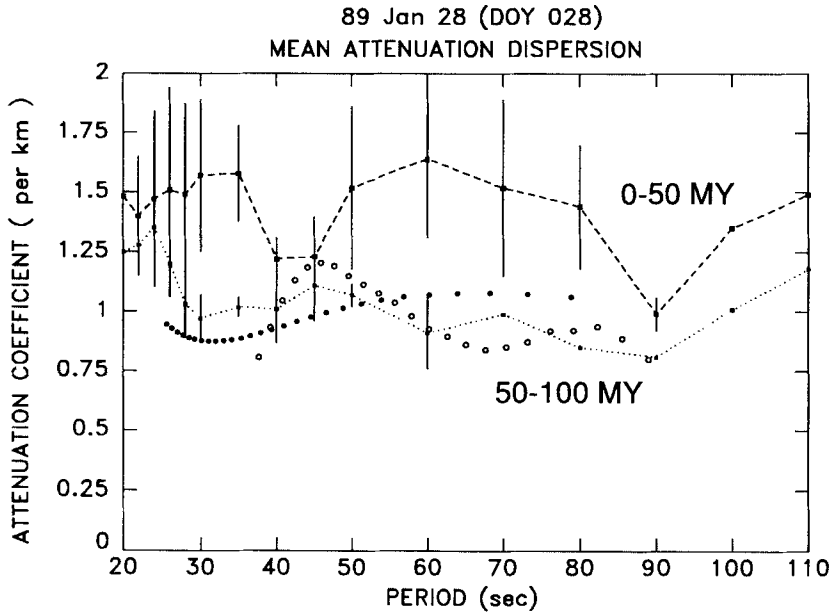

Figure 8. Summary of attenuation dispersion test. Two estimates of γ are compared with pure-path reference curves for two age provinces: $0 \leq t \leq 50$ Myr (dashed line), and $50 \leq t \leq 110$ Myr (dotted line). Open circles are measurements made from raw spectral ratios; filled circles are measurements made from interstation path responses derived with the Wiener filters.

As mentioned above, seismic refraction and reflection surveys have yielded reliable estimates of h_c throughout the study area. Along the Hawaiian Ridge, h_c varies from about 15 km near O'ahu and Hawai'i to about 9 km at Midway (Furumoto *et al.* 1968; Lindwall 1988). The thick crust represents the volcanic edifices produced by the hotspot, and is restricted to a width of $\sim$250 km. Off the ridge, refraction surveys indicate crust only one-half as thick, $h_c \sim 7.5$ km (Furumoto *et al.* 1971). The problem for this investigation is whether the interstation propagation paths sampled only the thick crust along the Hawaiian Ridge or some average of the thickened and normal crust. Again, the 30 s lower limit of the U and C dispersion curves drastically reduces the model resolution at crustal depths, but the effects of different values of h_c are not negligible. Therefore, in the following inverse models we considered two cases: $h_c = 7.5$ km and $h_c = 15$ km. The resulting models can be understood as 'end-members' that bound the true velocity structure. As we shall demonstrate, the assumption of either value for h_c does not change the conclusion that the total lithospheric thickness, h_l, is about 100 km.

Test of the thin-lithosphere hypothesis

The results of the first inversion are listed in Table 4, where layer thicknesses, starting and final values of β_V, calculated errors, and estimates of the vertical extent of the resolving kernel for each layer are provided. The starting model consisted of an ocean layer, a single-layer crust, a high-velocity upper-mantle lid, and a three-layer LVZ overlying a half-space. This parametrization differs from that used by Woods *et al.* (1991) only in that h_c was increased from 6 to 7.5 km. The model is illustrated in Fig. 9, where the starting model is shown as the dotted line and the final result as the solid line. As in our preliminary study, to match the observations the shear velocity in the uppermost layer of the LVZ (model layer 4, or ml-4) had to increase more than 1-σ, from 4.20 km s^{-1} to 4.54 ± 0.06 km s^{-1}. This value is consistent with those characteristic of the high-velocity lid. In contrast to the earlier results, the values in ml-5 and ml-6 exhibited changes of opposite sign: the shear velocity of ml-5 decreased slightly, from 4.20 to 4.12 ± 0.14 km s^{-1}, but the value in ml-6 increased from 4.20 to 4.38 ± 0.26 km s^{-1}. Both of these values remain, however, within 1-σ of the starting value of 4.20 km s^{-1}.

The accompanying resolving kernels demonstrate that the dispersion curves covered a sufficiently wide bandwidth so that, with this model parametrization, the velocity structure could be resolved down to $z \sim 200$ km. The kernels for ml-3, ml-4, and ml-5 had large amplitudes and were compact. The kernel for ml-6 was only slightly broader, indicating that some information from ml-5 and ml-7 contributed to the estimate of β_V at that depth. Moreover, with this model parametrization, there was little trade-off between the crust and upper-mantle velocities or between those of the lid and the LVZ. If h_l along the Hawaiian Swell had been reduced as much as required by the rejuvenation model ($h_l \sim 50$ km), our data should have sensed the transition between the lithosphere and the asthenosphere easily. Based on this inversion, we conclude that h_l cannot be as thin as 50 km.

Table 4. Inversion test of thinned-lithosphere hypothesis.

Layer ml_i	h_i (km)	β_V^{start} (km s^{-1})	β_V^{final} (km s^{-1})	σ (km s^{-1})	w_k (km)
1	4.5	0.00	0.00	0.02	7
2	7.5	3.90	3.98	0.02	8
3	50.0	4.50	4.58	0.02	50
4	50.0	4.20	4.54	0.06	50
5	50.0	4.20	4.12	0.14	50
6	50.0	4.20	4.38	0.26	50
7	---	4.55	4.67	0.11	---

Inversions with normal-thickness crust

We next explore the model space to find the best possible estimate of h_l, following the procedures outlined above. Two velocity models constructed with the assumption of normal-thickness crust are summarized in Table 5 and are illustrated in Fig. 10.

Fig. 10(a) shows the velocity model obtained with a detailed parametrization of the model space. As seen, the model achieves a good fit to the observed group and phase velocities over all periods and reveals a typical upper-mantle profile: a high-velocity lid above a low-velocity zone. The model is a relatively smooth, unbiased representation of the shear velocity structure that is required by the observations. Note that in this model the crustal shear velocity does not change significantly, although the resolving kernel at that depth is poor. Below the crust, ml-3 to ml-8 display compact, relatively large-amplitude resolving kernels. Resolution then degrades markedly for $z \geq 150$ km.

Based on the values of β_V and σ, the mantle lid in the current model consists of ml-3 to ml-7 and possibly ml-8. Of these layers, the greatest departure from the starting velocity occurs in ml-5 and ml-6, for which β_V increases to 4.63 ± 0.09 km s^{-1}. In ml-8, the velocity decreases to 4.43 ± 0.07 km s^{-1}, but this value is within 1-σ of the starting value. Including ml-8 in the lid, the cumulative thickness is 90 km, so, with the crust, the total lithospheric thickness, h_l, is 97.5 km. Because the shear velocity of ml-8 decreases, it might be considered to be part of the LVZ rather than the lid, but even if this is the case, $h_l = 82.5$ km, about 30 km thicker than demanded by the rejuvenation hypothesis.

Combining ml-3 to ml-8 into a single-layer mantle lid, and ml-9 to ml-14 into the LVZ yields the simplified model shown in Fig. 10(b). Of several inversions with such layer combinations and normal-thickness crust, this model offers the smallest RMS error between the calculated and observed dispersion curves. Decreasing h_l, say by only 10 per cent, degrades the overall inverse solution. For periods $T < 40$ s and $T > 60$ s the calculated dispersion values no longer fit the observations at the 1-σ level, and the RMS error increases by a factor of 5. In those cases, moreover, the trade-off between β_{LID} and β_{LVZ} results in implausibly high values of β_{LID} (e.g. ~ 5.2 km s^{-1}), contradicting the results from the seismic refraction surveys. In addition, β_{LVZ} increases to within 2 per cent of the starting value, effectively eliminating a well-developed LVZ.

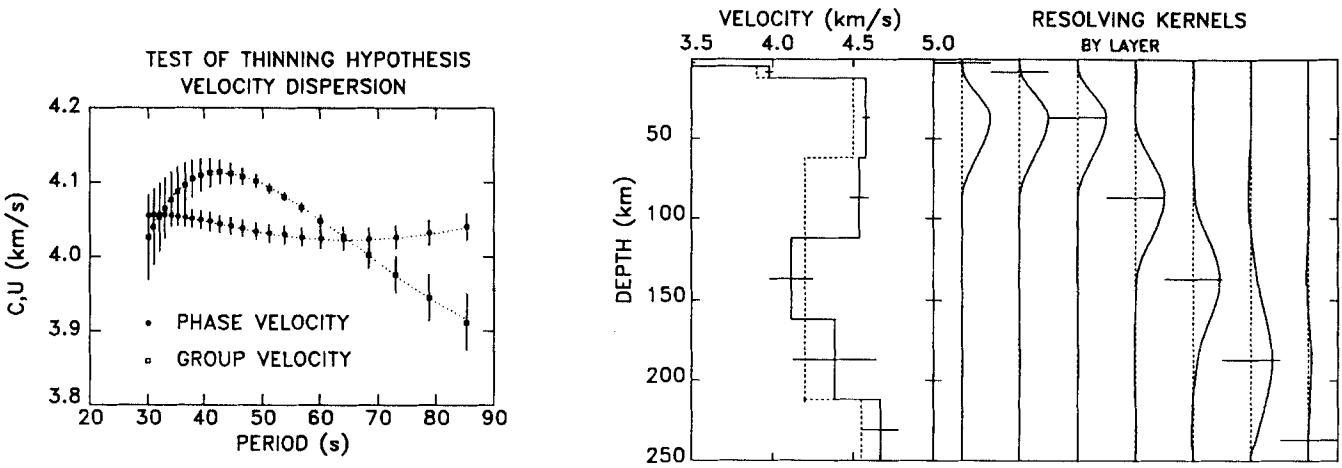

Figure 9. Summary of trial shear-velocity model for Hawaiian Swell. *Left.* Open squares represent group velocities; filled circles represent phase velocities; error bars are one standard error; dashed lines are inverse fits to observations. *Right.* In the velocity model the dashed line represents the starting values and the solid line represents the final values. Resolving kernels are normalized to the maximum value, and demonstrate that only the lithosphere (ml-3 and ml-4) is well resolved. The solution is particularly insensitive to the ocean and crust (ml-1 and ml-2). The large change between the starting and final velocities for ml-4 suggests thick lithosphere between Midway and O'ahu.

Table 5. Inverse models for β_V. Hawaiian Swell with Normal Crust.

layer ml_i	h_i (km)	β_V^{start} (km s^{-1})	β_V^{final} (km s^{-1})	σ (km s^{-1})	w_k (km)
		Detailed Parameterization			
1	4.50	0.00	0.00	0.00	52
2	7.50	3.90	3.92	0.16	52
3	15.00	4.50	4.52	0.16	52
4	15.00	4.50	4.56	0.05	53
5	15.00	4.50	4.63	0.09	56
6	15.00	4.50	4.63	0.09	58
7	15.00	4.50	4.55	0.06	58
8	15.00	4.50	4.43	0.07	59
9	15.00	4.50	4.33	0.08	62
10	15.00	4.50	4.25	0.08	69
11	15.00	4.50	4.22	0.08	77
12	15.00	4.50	4.23	0.09	84
13	15.00	4.50	4.27	0.12	90
14	15.00	4.50	4.33	0.14	94
15	15.00	4.50	4.41	0.14	98
16	15.00	4.50	4.50	0.11	102
17	15.00	4.50	4.59	0.07	106
18	---	4.50	4.67	0.12	---
		Simplified Parameterization			
1	4.50	0.00	0.00	0.00	29
2	7.50	3.90	3.98	0.01	29
3	90.00	4.50	4.58	0.01	90
4	90.00	4.50	4.21	0.01	90
5	---	4.50	4.64	0.03	---

Inversions with thick crust

Table 6 summarizes two models obtained following the same exploratory procedure used above but with the assumption of thick crust along the propagation paths. The models are illustrated in Fig. 11.

With the detailed parametrization (Fig. 11a), it is clear that the thick-crust inversion departs more from the starting model than does the normal-crust inversion. For example, the crustal shear velocity increases from 3.90 to 4.02 ± 0.13 km s^{-1}, but again the resolution at this depth is poor. Similarly, the velocities in ml-3, ml-4, ml-5, and ml-6 increase from their starting value of 4.5 km s^{-1} to about 4.62 km s^{-1}, while that in ml-7 remains virtually unchanged. The velocity in ml-8 decreases, however, to 4.41 ± 0.08 km s^{-1}, but this value is within 1-σ of the starting value. Deeper in the mantle, the velocities comprising the LVZ agree with the values in the normal-crust model to within 0.5 per cent. The important point to note is that the integrity of the lid is maintained; it shows no evidence of thinning, and we estimate that $h_{LID} \sim 90$ km. Adding the crust to this value then yields $h_l \sim 105$ km.

The simplified version of the thick-crust inverse model is shown in Fig. 11(b). As previously, the discontinuities were placed to reflect the gradients in the detailed parametrization, and the discontinuities being fixed as shown here minimized the RMS error between the observed and calculated dispersion. Again the model produces an excellent fit to the observations. Comparison of the simplified models for normal-thickness and thickened crust shows that they are very similar, differing on average by less than 1.5 per cent in the velocities at all depths.

DISCUSSION

The simplest interpretation of the inverse models presented above is that the lithosphere along the Hawaiian Swell between Midway Atoll and O'ahu has not been significantly thinned by the hotspot. Caution is warranted, however, because the models were restricted to *isotropic* shear velocities, and, as has been demonstrated repeatedly, the velocity structure of the oceanic lithosphere is *anisotropic*.

Lévêque (1991) has argued, for example, that the low velocities predicted along the swell by the rejuvenation model

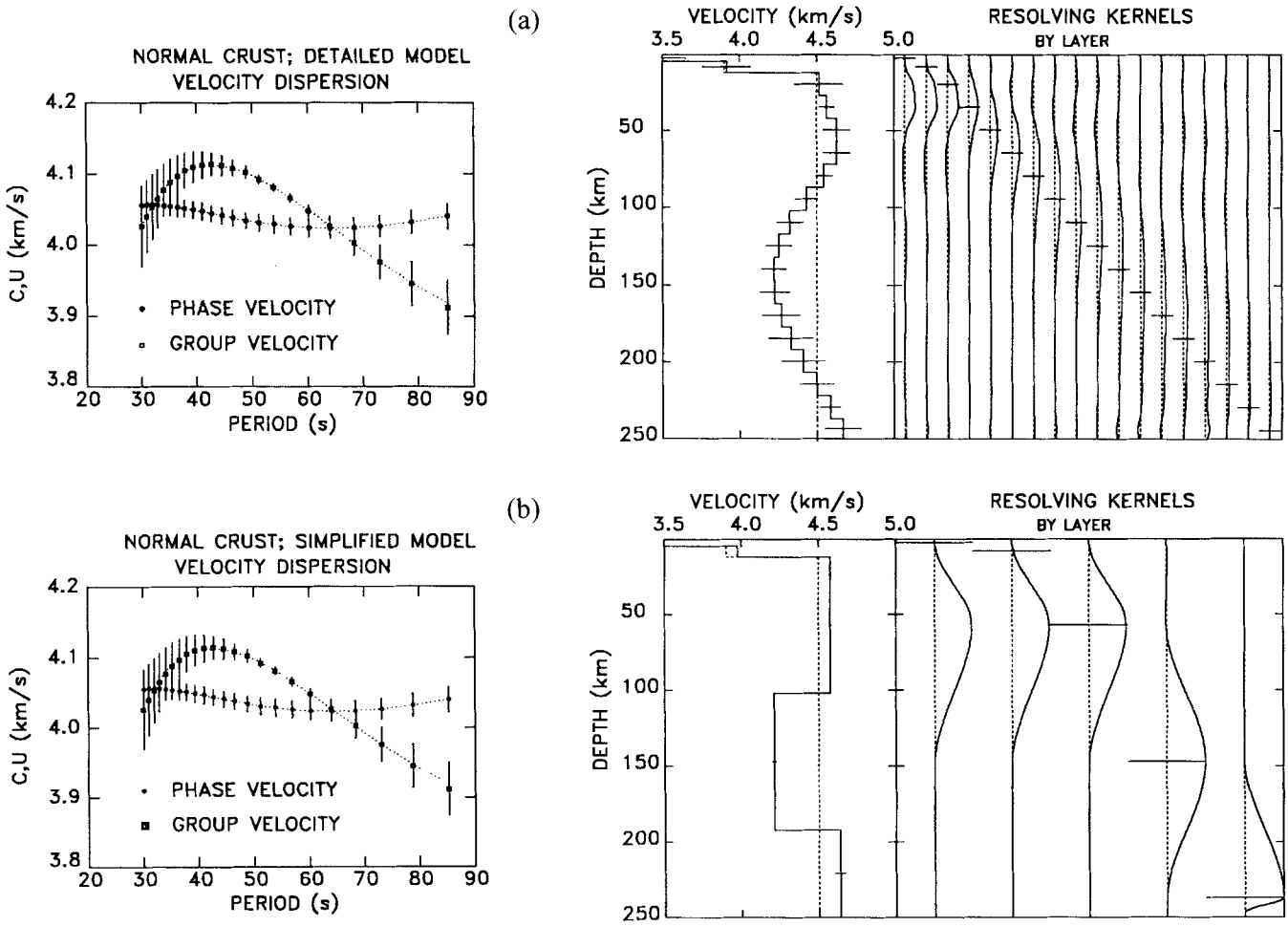

Figure 10. (a) Summary of detailed shear-velocity model for Hawaiian Swell with normal-thickness crust. *Left.* Open squares represent group velocities; filled circles represent phase velocities; error bars are one standard error; dashed lines are inverse fits to observations. *Right.* In the velocity model the dashed line represents the starting values and the solid line represents the final values. Resolving kernels are normalized to the maximum value, and show that β_V is reasonably well resolved to depths of $z \sim 150$ km. (b) As (a), but for the simplified shear-velocity model. Here β_V is reasonably well resolved at all depths.

might be masked by the effects of anisotropy. His interpretation is based on anisotropic (transversely isotropic) inverse models which assume that the fast *a*-axes of the olivine crystals [100] in the lithosphere are parallel to *fossil* plate directions and that the *a*-axes in the asthenosphere are parallel to *current* plate velocities in the hotspot reference frame. The difference between these directions at the Hawaiian Swell is about 45°. His results are, however, equivocal. When he assumed an initially thin lithosphere, inverting the interstation *C* dispersion curve yielded a thin lithosphere. When he assumed an initially thick lithosphere, however, h_l changed by less than 20 per cent from its starting value. This uncertainty reflects the trade-offs between lithospheric thickness and the angle to which the *a*-axes may have been reoriented by the hotspot. Given the difficulties in assessing these trade-offs, we think that measurements of attenuation might ultimately provide less ambiguous information about the presence of asthenosphere at depths of 50–70 km.

The comparison of the interstation measurements of *U* and *C* with the anisotropic pure-path reference curves in Fig. 7 is quite favourable, however; there appears to be little reason to invoke any reorientation of the crystal axes. The conclusion that $h_l \sim 100$ km therefore remains tenable. It also appears to be supported by the surface-wave tomographic images of the Pacific Basin constructed by Zhang & Tanimoto (1989, 1991). These images, which are also transversely isotropic, revealed a low-velocity zone in the vicinity of Hawai'i only; there was no low-velocity anomaly extending north-west along the swell.

Two body-wave studies offer tentative support to our contention that the lithosphere along the swell has not been significantly thinned. First, Sipkin & Jordan (1980) noted that traveltime residuals were negligible for multiple *ScS* phases that had bounce points along the swell's northern flank, an observation which suggests a normal shear-velocity structure. More recently, Bock (1991) examined precursors to *S* recorded by station HON on O'ahu, and identified them as *Sp* converted waves. Modelling the *S–Sp* residuals, he concluded that $70 \leq h_l \leq 80$ km. This estimate is intermediate between the value predicted by the rejuvenation model and the value determined in this investigation from the surface-wave analyses, but it is interesting to note that the upper limit is consistent with the mature plate thickness estimated by Stein & Stein (1992, $h_l = 95 \pm 15$ km). Also interesting is that Bock required that the contrast in shear velocity between the mantle lid ($\beta =$

Table 6. Inverse models for β_V. Hawaiian Swell with thick crust.

Layer ml_i	h_i (km)	β_V^{start} (km s^{-1})	β_V^{final} (km s^{-1})	σ (km s^{-1})	w_k (km)
		Detailed Parametrization			
1	4.50	0.00	0.00	0.00	51
2	15.00	3.90	4.02	0.13	51
3	15.00	4.50	4.62	0.13	51
4	15.00	4.50	4.63	0.05	53
5	15.00	4.50	4.63	0.10	55
6	15.00	4.50	4.59	0.08	57
7	15.00	4.50	4.51	0.06	58
8	15.00	4.50	4.41	0.08	61
9	15.00	4.50	4.33	0.08	67
10	15.00	4.50	4.26	0.08	74
11	15.00	4.50	4.24	0.08	80
12	15.00	4.50	4.25	0.10	86
13	15.00	4.50	4.29	0.13	91
14	15.00	4.50	4.36	0.14	96
15	15.00	4.50	4.44	0.14	99
16	15.00	4.50	4.53	0.10	103
17	15.00	4.50	4.61	0.07	106
18	---	4.50	4.69	0.13	---
		Simplified Parametrization			
1	4.50	0.00	0.00	0.00	36
2	15.00	3.90	4.02	0.01	36
3	75.00	4.50	4.62	0.01	75
4	105.00	4.50	4.28	0.01	105
5	---	4.50	4.63	0.03	---

4.60 km s^{-1}) and the LVZ (β=3.91 km s^{-1}) be 15 per cent. For the models presented here, the velocity contrast never exceeds 9 per cent. Thus, the results from surface waves and body waves appear to be inconsistent with one another, but because the surface waves yield an average structure over the 2100 km propagation path while the body waves offer a local estimate, perhaps this is not the case. It seems possible that any short-wavelength variation of h_1 directly beneath the islands comprising the archipelago might reflect ancient magma feeder zones, but not the broader-scale thinning postulated in the rejuvenation model. In other words, lithospheric thinning may occur but be very localized. In any case, Vinnik & Romanowicz (1991) have cautioned that precursors to *S*, such as those studied by Bock, may actually be generated by *S*-to-*P* and *P*-to-*P* scattering. Clearly, more measurements of *S*-precursors should be attempted, both at O'ahu and at Midway to settle this question.

The rejuvenation model encounters further difficulties as new geophysical data accumulate. For example, in early heat-flow measurements made along the swell's longitudinal axis, Von Herzen *et al.* (1982) identified a positive anomaly ($\sim$12 mW m^{-2}) and interpreted it to result from the conduction of the plume's heat pulse to the surface. This anomaly appeared about 700 km ESE of Midway, at the position of maximum surface expression predicted by the rejuvenation model, and so has often been cited as support for the model (e.g. Menard & McNutt 1982; Schroeder 1984). However, when Von Herzen *et al.* (1989) measured heat flow along a profile transverse to the swell's axis (specifically to verify the older measurements) they observed no systematic variation of heat flow that could be correlated with the swell. After re-evaluating their earlier results, they concluded that the anomalous heat flow associated with the Hawaiian Swell is less than 10 mW m^{-2}, and may not exist at all, given the scatter of the measurements. It seems, therefore, that heat flow measurements, which once were taken as supporting the rejuvenation model, must now be interpreted as refuting it or at best as equivocal.

Petrological data constrain the depth of origin of Hawaiian lavas. Such information should not be overlooked when discussing geophysical models, but the literature on this subject is extensive and cannot be discussed in detail here. Reviews are offered by Feigenson (1986), Frey & Roden (1987), and more recently by Wright & Clague (1989). In summary, the available radiogenic isotope, trace element, and transition metal data appear to be inconsistent with the hypothesis that the oceanic lithosphere undergoes significant remelting, and, in particular, the geochemical and geobarometry data available for Hawaiian lavas require that their source depth be within the garnet-lherzolite stability field, which must be deeper than 60 km.

If the rejuvenation model is incompatible with a growing body of observational data, alternative explanations for the formation of midplate swells, and the Hawaiian Swell in particular, will have to be re-examined and explored in detail. Recent theoretical work suggests that it is the buoyancy flux, *B*, of a mantle plume that controls the height and shape of swells, and that convective erosion of the lithosphere is not necessary for their formation. For example, Ribe & Christensen (1994) modelled the Hawaiian plume–lithosphere interaction with a 3-D fluid flow calculation. They found that, for an assumed temperature contrast of 300 K between the ascending plume and surrounding mantle, a *B* of 4100 kg s^{-1} produced a good fit to the observed swell bathymetry in vertical and horizontal cross-sections without any plume-induced erosion of the lithosphere's underside.

Using a parametrized convection model Sleep (1994) showed that the erosional thinning envisioned by the thermal rejuvenation model would require vigorous convection in the plume material ponded at the lithosphere's base, but such convection would inhibit the intrusion of warm, buoyant material into the lithosphere upstream from the plume, thus preventing the rapid inflation of the swell. Moreover, the vigour of the convection would require implausibly low values of viscosity (a reduction of the ambient value by a factor of 3×10^6). Although the presence of a low-viscosity layer beneath the Hawaiian Swell can reconcile the estimates of thermal and elastic lithosphere thickness (Robinson & Parsons 1988), the required reduction factor is much lower (1–2 orders of magnitude).

Davies (1994) agreed that beneath broad, midplate swells the lithosphere is unlikely to be thinned by thermomechanical erosion. He showed, however, that rapid erosion can occur directly above a *narrow* plume conduit, even if viscosity is reduced only slightly. Indeed, the plume radius, which defines the lateral scale of the uplift, appears to control the degree of erosion; in one experiment with a plume radius of 35 km, the geotherm intersected the dry mantle solidus in about 2 Myr. This result is consistent with those of Bock (1991) and Zhang

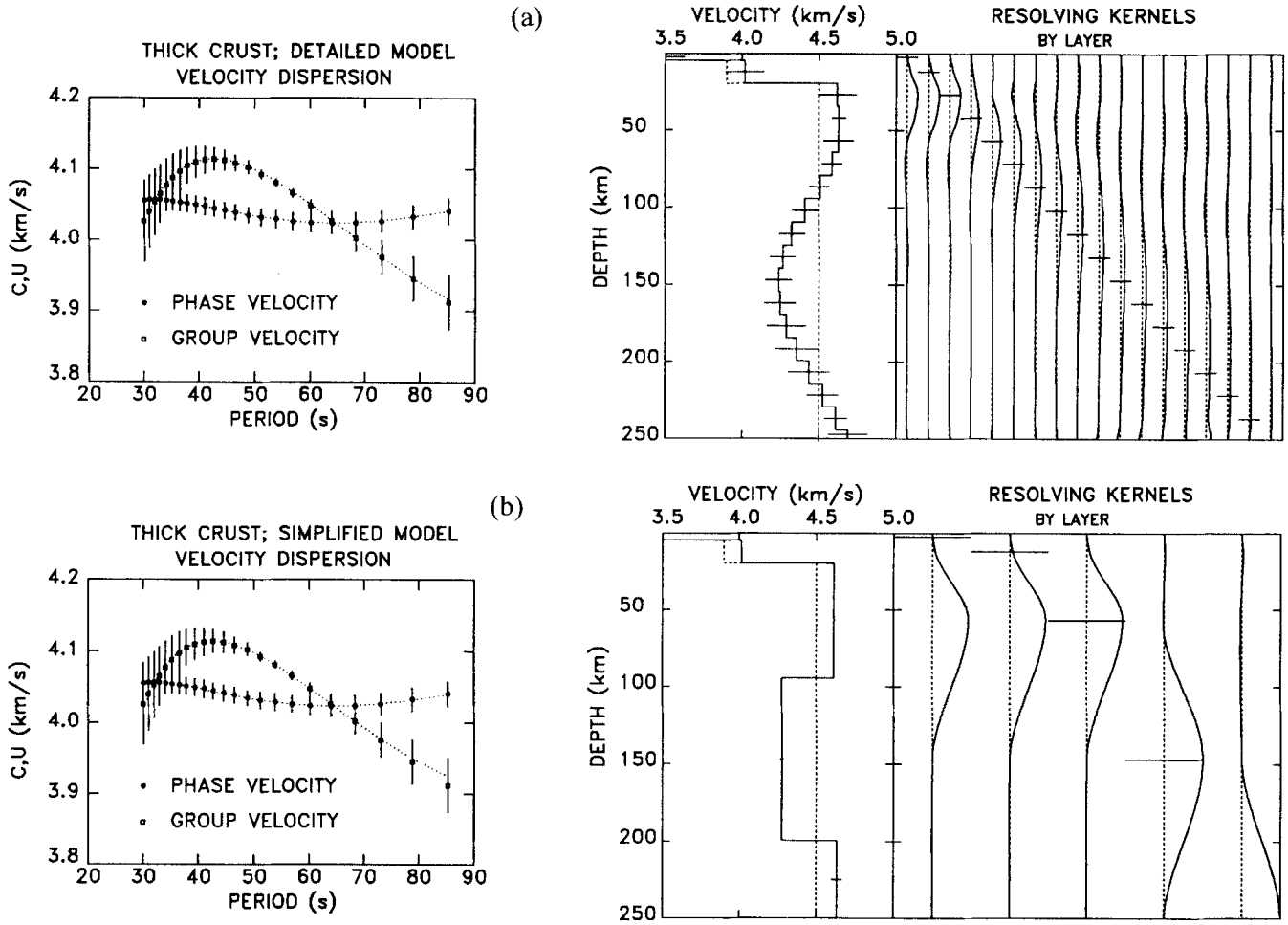

Figure 11. (a) Summary of detailed shear-velocity model for Hawaiian Swell with thick crust along Hawaiian Ridge. *Left.* Open squares represent group velocities; filled circles represent phase velocities; error bars are one standard error; dashed lines are inverse fits to observations. *Right.* In the velocity model the dashed line represents the starting values and the solid line represents the final values. Resolving kernels are normalized to the maximum value, and show that β_V is reasonably well resolved to depths $z \sim 150$ km. As (a) but for the simplified shear-velocity model. Here, β_V is reasonably well resolved at all depths.

& Tanimoto (1989, 1992), discussed earlier, which suggested only localized thinning directly beneath the Hawaiian islands.

A common feature of the three theoretical studies just discussed is a plume radius much narrower ($35 \leq r \leq 91$ km) than we assumed at the outset ($r \sim 500$ km) of this investigation. If the Hawaiian plume is this narrow, then the long-wavelength surface waves used in this study may indeed have failed to sense any localized thinning. Localized thinning is not, however, the widespread and drastic erosion demanded by the classic rejuvenation model and which our experiments were designed to detect. It remains reasonable, therefore, to state that the average thickness of the oceanic lithosphere along the Hawaiian Swell is not detectably thinner than mature, unperturbed lithosphere.

SUMMARY AND CONCLUSIONS

In this paper, we have presented two-station measurements of three Rayleigh-wave observables along the Hawaiian Swell: group velocity, phase velocity, and anelastic attenuation. These measurements, when compared with pure-path dispersion curves characterizing lithosphere for which $20 \leq t_c \leq 50$ Myr and $50 \leq t_c \leq 110$ Myr, suggest that the dispersion of the observables along the swell is a function of t_c and not of the thermally rejuvenated age t_{th} suggested by Detrick & Crough (1978). Shear-velocity models constructed for the swell by joint inversion of the dispersion curves all indicate that the lithosphere is ~ 100 km thick between Midway Atoll and O'ahu. This value is difficult to reconcile with the value of 40–50 km required by the classical rejuvenation model.

ACKNOWLEDGMENTS

We thank Jean-Jacques Lévêque for many valuable discussions about these experiments, and Daniel Rouland, Chantal Condis, Alfred Muller, and Jean-Michel Cantin, all of the IPG Staff in Strasbourg, France, for engineering and data support. We also thank the US Naval and civilian personnel on Midway for their interested cooperation and assistance in maintaining the station equipment. Don Forsyth and Norm Sleep helped sharpen our presentation with their careful reviews. this research was funded in part by ONR, under contract N-00014-89-J-1663, and by CNRS (NSF-CNRS grant 06943 and the INSU–GEOSCOPE program).

REFERENCES

Betz, F. & Hess, H.H., 1942. The floor of the north Pacific Ocean, *Geog. Rev.*, **32,** 99–116.

Bock, G., 1991. Long-period S to P converted waves and the onset of partial melting beneath Oahu, Hawaii, *Geophys. Res. Lett.*, **18,** 869–872.

Canas, J.A. & Mitchell, B.J., 1978. Lateral variation of surface-wave anelastic attenuation across the Pacific, *Bull. seism. Soc. Am.*, **68,** 1637–1650.

Cande, S.C., LaBrecque, J.L., Larson, R.L., Pitman, III, W.C., Golovchenko, X. & Haxby, W.E., 1969. Magnetic Lineations of the World's Ocean Basins, *AAPG Map,* AAPG, Tulsa, OK.

Clague, D.A. & Dalrymple, G.B., 1989. Tectonics, geochronology, and origin of the Hawaiian–Emperor volcanic chain, in *The Geology of North America: The Eastern Pacific Ocean and Hawaii, N,* pp. 188–217, eds. Winterer, E.L., Hussong, D.M. & Decker, R.W., GSA, Boulder, CO.

Crough, S.T., 1978. Thermal origin of mid-plate hot-spot swells, *Geophys. J. R. astr. Soc.*, **55,** 451–469.

Crough, S.T., 1983. Hotspot swells, *Ann. Rev. Earth planet. Sci.*, **11,** 165–193.

Dalrymple, G.B., Clague, D.A. & Lanphere, M.A., 1977. Revised age for Midway volcano, Hawaiian volcano chain, *Earth planet. Sci. Lett.*, **37,** 107–116.

Davies, G.F., 1994. Thermomechanical erosion of the lithosphere by mantle plumes, *J. geophys. Res.*, **99,** 15 709–15 722.

Der, Z.A. & Landisman, M., 1972. Theory for errors, resolution, and separation of unknown variables in inverse problems, with application to the mantle and the crust in southern Africa and Scandinavia, *Geophys. J. R. astr. Soc.*, **27,** 137–178.

Detrick, R.S. & Crough, S.T., 1978. Island subsidence, hot spots, and lithospheric thinning, *J. geophys. Res.*, **83,** 1236–1244.

Detrick, R.S., von Herzen, R.P., Crough, S.T., Epp, D. & Fehn, U., 1981. Heat flow on the Hawaiian swell: A test of the lithospheric reheating model, *Nature,* **292,** 142–143.

Doell, R. & Dalrymple, G.B., 1973. Potassium–Argon ages and paleomagnetism of the Waianae and Koolau volcanic series, Oahu, Hawaii, *Geol. Soc. Am. Bull.*, **84,** 1217–1241.

Epp, D., 1984. Implications of volcano and swell heights for thinning of the lithosphere by hotspots, *J. geophys. Res.*, **89,** 9991–9996.

Feigenson, M.D., 1986. Constraints on the origin of Hawaiian lavas, *J. geophys. Res.*, **91,** 9383–9393.

Forsyth, D.W., 1975. The early structural evolution and anisotropy of the oceanic upper mantle, *Geophys. J. R. astr. Soc.*, **43,** 103–162.

Frey, F.A. & Roden, M.F., 1987. The mantle source for the Hawaiian islands: Constraints from the lavas and ultramafic inclusions, in *Mantle Metasomatism,* pp. 423–463, eds Menzies, M. & Hawkesworth, C. Academic Press, Orlando, Fl.

Furumoto, A.S., Woollard, G.P., Campbell, J.F. & Hussong, D.M., 1968. Variation in the thickness of the crust in the Hawaiian archipelago, in *The Crust and Upper Mantle of the Pacific Area, Geophysical Monograph 12,* pp. 94–111, eds Knopoff, L., Drake, C.L. & Hart, P.J., AGU, Washington, DC.

Furumoto, A.S., Campbell, J.F. & Hussong, D.M. 1971. Seismic refraction surveys along the Hawaiian ridge, Kauai to Midway Island, *Bull. seism. Soc. Am.*, **61,** 147–166.

Herrin, E. & Goforth, T., 1977. Phase-matched filters: application to the study of Rayleigh waves, *Bull. seism. Soc. Am.*, **67,** 1259–1275.

Hwang, H.-J. & Mitchell, B.J., 1986. Interstation surface wave analysis by frequency-domain Wiener deconvolution and modal isolation, *Bull. seism. Soc. Am.*, **76,** 847–864.

Jackson, E.D. & Shaw, H.R., 1975. Stress fields in central portions of the Pacific plate: delineated in time by linear volcanic chains, *J. geophys. Res.*, **80,** 1861–1874.

Jackson, E.D. & Wright, T.L., 1970. Xenoliths in the Honolulu volcanic series, Hawaii, *J. Petrol.*, **11,** 405–430.

Kirkwood, S.C. & Crampin, S., 1981a. Surface wave propagation in an ocean basin with an anisotropic upper mantle: Numerical modeling, *Geophys. J. R. astr. Soc.*, **64,** 463–485.

Kirkwood, S.C. & Crampin, S., 1981b. Surface wave propagation in an ocean basin with an anisotropic upper mantle: Observations of polarization anomalies, *Geophys. J. R. astr. Soc.*, **64,** 487–497.

Leeds, A.R., 1975. Lithospheric thickness in the western Pacific, *Phys. Earth planet. Inter.*, **11,** 61–64.

Lévêque, J.J., 1991. Inversion of phase velocity data related to the Hawaiian Swell: Effect of anisotropy (abstract), *XX General Assembly IUGG IASPEI,* 87.

Lindwall, D.A., 1988. A two-dimensional seismic investigation of crustal structure under the Hawaiian Islands near Oahu and Kauai, *J. geophys. Res.*, **93,** 12 107–12 122.

Liu, M. & Chase, C.G., 1989. Evolution of midplate hotspot swells: numerical solutions, *J. geophys. Res.*, **94,** 5571–5584.

Maupin, V., 1992. Modelling of laterally trapped surface waves with application to Rayleigh waves in the Hawaiian swell, *Geophys. J. Int.*, **110,** 553–570.

McDougall, I., 1971. Volcanic island chains and sea floor spreading, *Nature Phys. Sci.*, **231,** 141–144.

Menard, H.W., 1973. Depth anomalies and the bobbing motion of drifting islands, *J. geophys. Res.*, **78,** 5128–5137.

Menard, H.W. & McNutt, M., 1982. Evidence for and consequences of thermal rejuvenation, *J. geophys. Res.*, **87,** 8570–8580.

Mitchell, B.J. & Yu, G.K., 1980. Surface wave dispersion, regionalized velocity models, and anisotropy of the Pacific crust and upper mantle, *Geophys. J. R. astr. Soc.*, **63,** 497–514.

Morgan, W.J., 1971. Convection plumes in the lower mantle, *Nature,* **230,** 42–43.

Morgan, W.J., 1972. Plate motions and deep mantle convection, *Geol. Soc. Am. Mem.*, **132,** 7–22.

Nishimura, C. & Forsyth, D., 1988. Rayleigh wave phase velocities in the Pacific with implications for azimuthal anisotropy and lateral heterogeneities, *Geophys. J. R. astr. Soc.*, **94,** 479–501.

Parsons, B. & Sclater, J.G., 1977. An analysis of the variation of ocean floor bathymetry and heat flow with age, *J. geophys. Res.*, **82,** 803–827.

Ribe, N. & Christensen, U.M., 1994. Three-dimensional modeling of plume-lithosphere interaction, *J. geophys. Res.*, **99,** 669–682.

Robinson, E.M. & Parsons, B., 1988. Effect of a shallow low-viscosity zone on the formation of midplate swells, *J. geophys. Res.*, **93,** 3144–3156.

Russell, D.R., Herrmann, R.B. & Hwang, H.-J., 1988. Application of frequency variable filters to surface wave amplitude analysis, *Bull. seism. Soc. Am.*, **78,** 339–354.

Sandwell, D.T. & Poehls, K.A., 1980. A compensation mechanism for the central Pacific, *J. geophys. Res.*, **85,** 3751–3758.

Sandwell, D.T. & Renkin, M.L., 1988. Compensation of swells and plateaus in the north Pacific: no direct evidence for mantle convection, *J. geophys. Res.*, **93,** 2775–2783.

Schroeder, W., 1984. The empirical age–depth relation and depth anomalies in the Pacific Ocean basin, *J. geophys. Res.*, **89,** 9873–9883.

Sipkin, S.A. & Jordan, T.H., 1980. Multiple ScS travel times in the western Pacific; implications for mantle heterogeneity, *J. geophys. Res.*, **85,** 853–861.

Sleep, N.H., 1994. Lithospheric thinning by midplate mantle plumes and the thermal history of hot plume material ponded at sublithospheric depths, *J. geophys. Res.*, **99,** 9327–9343.

Stein, C. & Stein, S., 1992. A model for the global variation in oceanic depth and heat flow with lithospheric age, *Nature,* **359,** 123–129.

Taylor, S.R. & Toksöz, M.N., 1982. Measurement of interstation phase and group velocity and Q using Wiener filtering, *Bull. seism. Soc. Am.*, **72,** 73–91.

US Naval Oceanographic Office, *DBDB5 bathymetric data,* National Geophysical Data Center, Boulder, CO.

Vig, P.K. & Mitchell, B.J., 1990. Anisotropy beneath Hawaii from surface wave particle motion observations, *Pageoph,* **133,** 1–22.

Vinnik, L.P. & Romanowicz, B.A., 1991. Origin of precursors to teleseismic S waves, *Bull. seism. Soc. Am.*, **81,** 1216–1230.

Von Herzen, R.P., Detrick, R.S., Crough, S.T., Epp, D. & Fehn, U., 1982. Thermal origin of the Hawaiian swell: Heat flow evidence and thermal models, *J. geophys. Res.*, **87,** 6711–6723.

Von Herzen, R.P., Cordery, M.J., Detrick, R.S. & Fang, C., 1989. Heat flow and the thermal origin of hotspot swells: the Hawaiian swell revisited, *J. geophys. Res.*, **94,** 13 783–13 799.

Wessel, P., 1993. Observational constraints on models of the Hawaiian hot spot swell, *J. geophys. Res.*, **98,** 16 095–16 104.

Wilson, J.T., 1963. A possible origin of the Hawaiian Islands, *Can. J. Phys.*, **41,** 863–870.

Woods, M.T. & Okal, E.A., 1994. The structure of the Nazca ridge and the Sala y Gomez seamount chain from the dispersion of Rayleigh waves, *Geophys. J. Int.*, **117,** 205–222.

Woods, M.T., Lévêque, J.-J., Okal, E.A. & Cara, M., 1991. Two-station measurements of Rayleigh wave group velocity along the Hawaiian swell, *Geophys. Res. Lett.*, **18,** 105–108.

Wright, T.L. & Clague, D.A., 1989. Petrology of Hawaiian lava, in *The Eastern Pacific Ocean and Hawaii, The Geology of North America N,* pp. 218–237, eds Winterer, E.L., Hussong, D.M. & Decker, R.W., Geol. Soc. Am., Boulder, CO.

Zhang, Y.S. & Tanimoto, T., 1989. Three-dimensional modelling of upper mantle structure under the Pacific Ocean and surrounding area, *Geophys. J. Int.*, **98,** 255–269.

Zhang, Y.-S. & Tanimoto, T., 1991. Global Love wave phase velocity variation and its significance to plate tectonics, *Phys. Earth planet. Inter.*, **66,** 160–202.

Zhu, A. & Wiens, D.A., 1991. Thermoelastic stress in oceanic lithosphere due to hotspot reheating, *J. geophys. Res.*, **96,** 18 323–18 334.